

Synthesis, Structure and Properties of Compounds Derived from Kotoite-related Structures: $A_2MB_2O_6$ ($A = Zn, Ba, Pb$; $B = Pb, Ba, Zn, Cu$)

 Shreya Sasmal,^[a] Nainamalai Devarajan,^[a] and Srinivasan Natarajan*^[a]

A series of compounds with the general formula $A_2MB_2O_6$ ($A=Zn, Ba, Pb$; $B=Pb, Ba, Zn, Cu$) related to the kotoite structure has been prepared employing high-temperature solid state methods. The substitution of transition elements in place of Zn^{2+} ions resulted in colored compounds. The optical absorption spectra could be explained based on Tanabe-Sugano diagram and allowed d-d transitions. Dielectric studies on $Ba_2ZnB_2O_6$, $(Ba_{1.5}Pb_{0.5})ZnB_2O_6$, $PbZn_2B_2O_6$, $Pb_{1.5}Zn_{1.5}B_2O_6$, $BaZn_2B_2O_6$ and $Pb_2CuB_2O_6$ at room temperature indicate

reasonable values at low frequencies, which decrease on increasing frequencies. Magnetic study of synthesized single-phase compounds $BaZnCoB_2O_6$ and $Pb_2CuB_2O_6$ have been performed. The substitution of Eu^{3+} , Tb^{3+} and Tm^{3+} in place of Ba^{2+} in $Ba_2ZnB_2O_6$, gives rise to the expected emission of red, green and blue colors. Suitable modifications of the different phosphors in $Ba_2ZnB_2O_6$, resulted in white-light emission in $Ba_2ZnB_2O_6$. The $Pb_2CuB_2O_6$ compound was found to be a good catalyst in the ipso-hydroxylation of arylboronic acids.

Introduction

Of the many compounds known within the realm of minerals, those of borates is important.^[1] The borates have interesting structures originating from the different coordination number and geometry: 3-coordinated trigonal planar and 4-coordinated tetrahedral boron.^[2] In addition, it has been noted that boron readily forms B–O–B bonds that results in many variants of borate units within the structure.^[3] One of the characteristics of the borate structures is that it adopts non-centrosymmetric space groups more readily compared to phosphate and silicate-based structures. The non-centrosymmetric nature of the borates has been exploited towards non-linear optical (SHG) and laser applications.^[4]

Borates containing transition elements and lanthanides have been investigated for their magnetic and emission behaviour.^[5] It is also known that the presence of transition elements in the borate structures lead to interesting coloured compounds.^[6] Borates have also been explored as cathodes in battery materials.^[7] Of the many known anhydrous borate minerals, kotoite with the general formula $A_3(BO_3)_2$ is important.^[8] The structure generally has either tetrahedral or octahedral metal units connected by BO_3 trigonal planar units forming either a two-dimensional or a three-dimensional structure. We have recently explored the range of solid solubility in the kotoite related $Zn_3B_2O_6$ - $Co_3B_2O_6$ structures.^[9]

In continuation of this theme, we explored another kotoite related family of compounds with the general formula A_2M -

(B_2O_6) where $A=Zn, Ba, Pb$; $M=Cu, Zn, Ba, Pb$. The compounds $Ba_2ZnB_2O_6$ as well as $BaZn_2B_2O_6$ stabilizes in the non-centrosymmetric space groups, $Pca2_1$ ^[10] and $P2_12_12_1$ respectively.^[11] The compounds $Pb_2CuB_2O_6$ and $PbZn_2B_2O_6$ forms in centrosymmetric space groups $P2_1/c$ ^[12] and $Pccn$ respectively.^[13] These four compounds have not been explored for their properties except for the structural studies. We have taken up the investigation of these compounds to explore the effect of substitution at the Zn position by transition elements. In addition, we have also investigated the dielectric, luminescence including white-light emission and magnetic behaviour of these compounds. The compound, $Pb_2CuB_2O_6$, was studied as a heterogenous catalyst towards hydroxylation of aryl boronic acids. In this paper, we report the synthesis, evolution of colour, luminescence, dielectric, magnetic and heterogenous catalytic studies.

Results and Discussion

As part of the present study, we have investigated four different compounds $Ba_2ZnB_2O_6$ (1), $BaZn_2B_2O_6$ (2), $PbZn_2B_2O_6$ (3) and $Pb_2CuB_2O_6$ (4). All the structures are closely related to each other with differences in the coordination environment of the heavy metal atoms. Furthermore, the structures are stabilised in different space groups which offer considerable scope for investigating different properties.

Structure of 1, $Ba_2ZnB_2O_6$

The structure of 1 is formed by the connectivity between Ba^{2+} polyhedra, ZnO_4 tetrahedra and BO_3 triangles.^[10] The structure has zinc borate layers formed by the vertex-sharing between the ZnO_4 tetrahedra and the BO_3 triangles (Figure 1a). Within the zinc borate layers, each ZnO_4 tetrahedra is connected to

[a] S. Sasmal, N. Devarajan, S. Natarajan
 Solid State and Structural Chemistry Unit, Indian Institute of Science,
 Bangalore-560012, (India)
 E-mail: snatarajan@iisc.ac.in

Supporting information for this article is available on the WWW under
<https://doi.org/10.1002/asia.202400868>

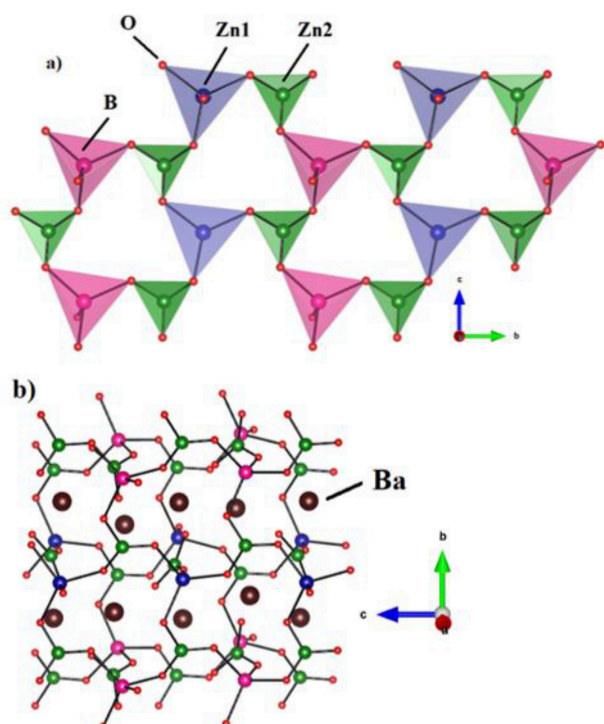


Figure 1. a) View of zinc borate layers b) The three-dimensional structure of $\text{Ba}_2\text{ZnB}_2\text{O}_6$.

three BO_3 units and each BO_3 units are connected to three ZnO_4 tetrahedra. This gives rise to the 6-membered apertures within the layer. The ZnO_4 tetrahedra are oriented up and down in the layer with the fourth oxygen connected with additional BO_3 units and Ba^{2+} ions forming the overall structure (Figure 1b).

The presence of ZnO_4 units in the structure provides an opportunity to examine the substitution of transition elements in place of Zn^{2+} ions. The substitution of Co^{2+} , Ni^{2+} and Cu^{2+} ions were attempted in place of Zn^{2+} ions in $\text{Ba}_2(\text{Zn}_{1-x}\text{M}_x)\text{B}_2\text{O}_6$ ($\text{M}=\text{Co}$, Ni and Cu). Partial substitution of these ions was successful. In all the cases, the maximum substitution was found to be $x=0.25$ by PXRD (ESI: Figure S1). Attempts to substitute higher concentrations resulted in a mixture of phases.

Structure of 2, $\text{BaZn}_2\text{B}_2\text{O}_6$

In the structure of 2, there are two one-dimensional chains—one formed by $\text{Zn}(1)\text{-O-B}$, which has 3-membered rings connected together and the other one-dimensional chains of $\text{Zn}(2)\text{-O-B}$ formed by 4-membered rings (Figure 2a and b).^[11] The connectivity between the two 1D chains give rise to a two-dimensional layer with 6-membered apertures (Figure 2c). Similar layer arrangements have been observed in many aluminophosphate structures.^[17] The layers are connected through the oxygens forming the 3D structure with voids. The Ba^{2+} ions occupy these voids (Figure 2d).

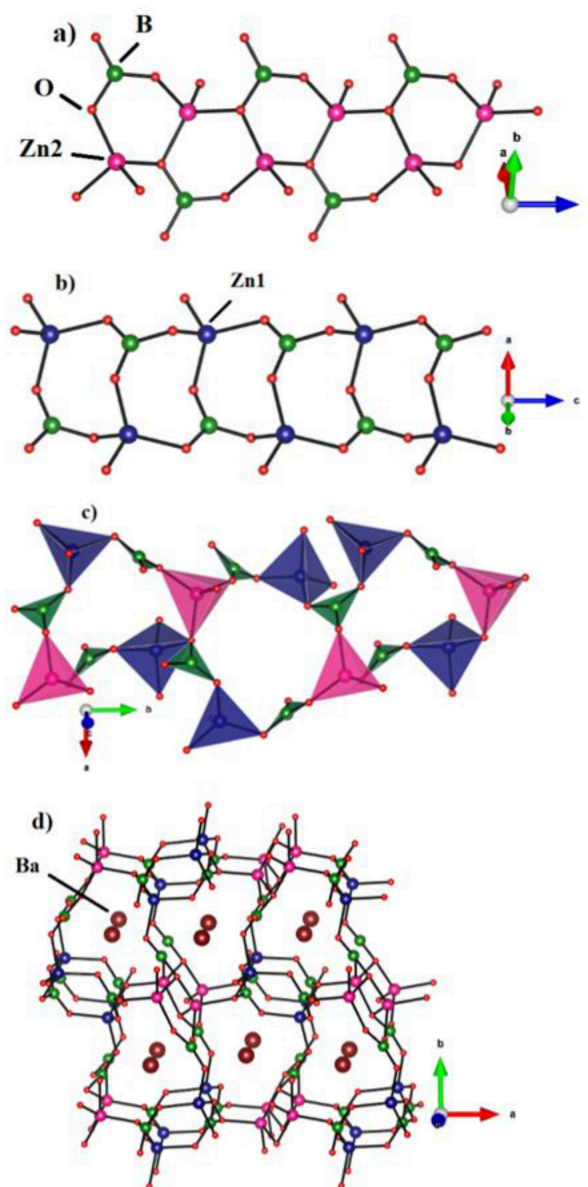


Figure 2. a) View of one-dimensional chains formed between $\text{Zn}(1)\text{-O-B}$ connectivity. Note that the chains are formed by 3-membered zinc borate rings. b) View of the second one dimensional chain, formed between $\text{Zn}(2)\text{-O-B}$ connectivity. Note that chains are formed by 4-membered zinc borate rings. c) Two-dimensional zinc borate layer. d) 3D structure of $\text{BaZn}_2\text{B}_2\text{O}_6$.

The structure of $\text{BaZn}_2\text{B}_2\text{O}_6$ is more amenable to substitution at the Zn^{2+} sites, possibly due to the availability of more tetrahedral positions. Thus, we have been successful in making single phase compounds of $\text{BaZn}_{2-x}\text{Co}_x\text{B}_2\text{O}_6$ ($0 < x \leq 1$), $\text{BaZn}_{2-x}\text{Ni}_x\text{B}_2\text{O}_6$ ($0 < x \leq 0.75$) and $\text{BaZn}_{2-x}\text{Cu}_x\text{B}_2\text{O}_6$ ($0 < x \leq 0.5$) (ESI: Figure S2). We have made attempts at refining the $\text{BaZnCoB}_2\text{O}_6$ structure employing Rietveld refinement protocols within GSAS II program. The refinement results are shown in ESI (Table S2 and Figure S3). Attempts to substitute higher concentrations of the transition metal ions in place of Zn^{2+} ions resulted in a mixture of phases, which are the different variants of the kotoite related structure.

Structure of 3, $\text{PbZn}_2\text{B}_2\text{O}_6$

The structure of **3** also has one-dimensional units formed by 3- and 4-membered rings. The one-dimensional chains are connected to form a two-dimensional zinc borate layer (Figure 3a). The Pb^{2+} ions connect the zinc borate layers, forming the 3D structure (Figure 3b). The position of the Pb^{2+} ions in this structure is such that the 6 s^2 lone pair of electrons are oriented in opposite directions.

Similar to **1** and **2**, we attempted to substitute Co^{2+} , Ni^{2+} and Cu^{2+} ions in place of Zn^{2+} ions in this structure as well. Our studies indicate that single phase compounds are realised for $\text{PbZn}_{2-x}\text{Co}_x\text{B}_2\text{O}_6$ ($0 < x \leq 0.75$) and $\text{PbZn}_{2-x}\text{Cu}_x\text{B}_2\text{O}_6$ ($0 < x \leq 0.5$) only (ESI, Figure S4). We were not successful in substituting Ni^{2+} ions in $\text{PbZn}_2\text{B}_2\text{O}_6$ compound. Higher substitution of Co^{2+} and Cu^{2+} ions in $\text{Pb}(\text{Zn}_{2-x}\text{M}_x)\text{B}_2\text{O}_6$ resulted in mixture of phases of different variants of kotoite structure.

Structure of 4, $\text{Pb}_2\text{CuB}_2\text{O}_6$

The structure of **4** consists of a copper borate layer formed by the connectivity between square planar CuO_4 and triangular BO_3 units that are connected by the Pb^{2+} ions. The CuO_4 and BO_3 moieties are connected together forming a layer formed by 8-membered rings (ESI: Figure S5a). These layer units are connected by 7-coordinated Pb^{2+} ions forming the three-dimensional structure (ESI: Figure S5b).

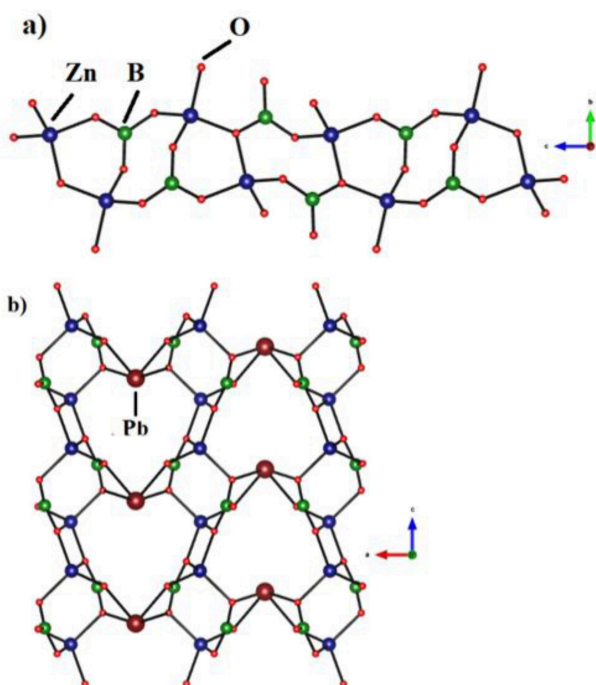


Figure 3. a) View of two-dimensional chains formed between Zn–O–B connectivity. Note that the chains are formed by 3-membered and 4-membered zinc borate rings. b) The three-dimensional structure of $\text{PbZn}_2\text{B}_2\text{O}_6$.

Our attempts at the substitution of Cu^{2+} ions by other ions including Co^{2+} and Ni^{2+} ions were not successful.

Structural Comparison

In the present study, we have taken up four different borate compounds that are related to the kotoite structure with the general formula $\text{A}_3\text{B}_2\text{O}_6$. The compounds $\text{Ba}_2\text{ZnB}_2\text{O}_6$ and $\text{BaZn}_2\text{B}_2\text{O}_6$ stabilises in the non-centrosymmetric space groups,^[10,11] whereas the Pb^{2+} containing ones, $\text{PbZn}_2\text{B}_2\text{O}_6$ and $\text{Pb}_2\text{CuB}_2\text{O}_6$ stabilises in a centrosymmetric space group.^[12,13] All the four compounds have metal borate layers that are connected differently giving rise to the three-dimensional structure. The metal borate layers in all the compounds are distorted and possess different types of voids. Thus, in compound **1**, the zinc borate layers have only 6-membered rings, compounds **2** and **3** have both 3- and 4-membered rings; and compound **4** have 8-membered rings. The differences in the structural arrangements along with the distortions at the metal centres (Zn-centre) resulted in partial substitution of the transition elements in all the structures. In compound **4**, the presence of the J–T distorted square planar Cu^{2+} ions could be the reason for not being able to substitute other transition elements in place of Cu^{2+} ions. The substitutions in compounds **1–3**, however, provided opportunities to investigate the evolution of colour in these compounds and compound **4** was found to be useful towards heterogenous catalysis.






























Optical Properties

In the present study, the partial replacement of Zn^{2+} ions by $\text{Co}^{2+}/\text{Ni}^{2+}/\text{Cu}^{2+}$ ions in the tetrahedral environment have been achieved. We investigated the evolution of colour as well as the associated optical properties of the transition metal substituted compounds.

The parent compounds **1**, **2** and **3** are white in colour. The substitution of Co^{2+} ions in the compounds exhibit different shades of blue colour in the case of compounds **1** and **2**. Compound **3**, on the other hand, gives rise to a deep blue, which turns to black colour on higher substitution (Table 1). It has been known that the presence of Co^{2+} ions in tetrahedral coordination give rise to blue colour.^[18–20]

The optical absorption spectra, (Figure 4a–c) at room temperature exhibit the expected triplet absorption band in the range of 450–730 nm (2.75–1.7 eV) for the tetrahedral Co^{2+} ions. The maxima at ~590 nm (2.1 eV) falls in the yellow-orange region and the complementary colour would be blue-purple.^[21] Normally, the Co^{2+} ions in tetrahedral coordination exhibits three spin-allowed transitions: (i) ${}^4\text{A}_2(\text{F}) \rightarrow {}^4\text{T}_2(\text{F})$, (ii) ${}^4\text{A}_2(\text{F}) \rightarrow {}^4\text{T}_1(\text{F})$ and (iii) ${}^4\text{A}_2(\text{F}) \rightarrow {}^4\text{T}_1(\text{P})$.^[22–24] The transitions (i) and (ii) are observed in the IR region and transition (iii) is observed in the visible region. Thus, the observed triplet band is assigned to the tetrahedral Co^{2+} ions [${}^4\text{A}_2(\text{F}) \rightarrow {}^4\text{T}_1(\text{F})$] transition. The additional transitions that have been observed for the compounds **2** and **3** may be due to the spin-forbidden transitions. Thus the peak at

Table 1. Compounds prepared in the present study under daylight.

Compound	x = 0.0	x = 0.1	x = 0.25	x = 0.5	x = 0.75	x = 1.0
Ba ₂ Zn _{1-x} Co _x B ₂ O ₆						
BaZn _{2-x} Co _x B ₂ O ₆						
PbZn _{2-x} Co _x B ₂ O ₆						
Ba ₂ Zn _{1-x} Ni _x B ₂ O ₆						
BaZn _{2-x} Ni _x B ₂ O ₆						
Ba ₂ Zn _{1-x} Cu _x B ₂ O ₆						
BaZn _{2-x} Cu _x B ₂ O ₆						
PbZn _{2-x} Cu _x B ₂ O ₆						

~440 nm (2.82 eV) observed in **2** can be assigned to the $^4A_2(F) \rightarrow ^2T_2(G)$ transition. Similarly, the peak at ~746 nm (1.66 eV) observed in **3** can be assigned to the $^4A_2(F) \rightarrow ^2E(^2G)$ transition.^[21]

The substitution of Ni²⁺ ions in the compounds exhibit colours that change from mint green to greenish yellow for **1** and **2** respectively (Table 1). As mentioned before, we were not successful in substituting Ni²⁺ ions in the structure of **3**. The optical absorption spectra for Ni²⁺ substituted compounds (Figure 5a and b) exhibit a triplet absorption band in the range 370–540 nm (3.39–2.28 eV). For the tetrahedral Ni²⁺ ions, the transitions: $^3T_1(F) \rightarrow ^3T_2(F)$, $^3A_2(F)$, and $^3T_1(P)$ ^[25,26] are allowed. Of these, the $^3T_1(F) \rightarrow ^3T_1(P)$ transition is the spin-allowed transition and is known to be observed in the visible region, which is the observed triplet bands. The weak absorptions observed at ~556 nm and ~718 nm for the Ni-substituted compounds in **1** and **2** may be due to the spin-orbit coupling. Similar bands

have been observed before for the d⁸-Ni²⁺ ions in the tetrahedral geometry. The Tanabe-Sugano diagram for the tetrahedral d⁷ (Co²⁺) and d⁸ (Ni²⁺) ions are given in ESI (Figure S6).

The copper substitutions in the compounds result in different shades of blue for **2** and **3** and a grey colour for **1** (Table 1). It has been shown that Cu²⁺ ions in tetrahedral coordination exhibits a broad absorption.^[21] The optical absorption spectra (Figure 6a–c) for the compounds **2** and **3** exhibits an absorption that starts from ~2.4 eV (516 nm) and extends into the near-IR region. The main absorption can be assigned to the $^2T_2 \rightarrow ^2E_2$ transition.^[21] The optical spectra of Cu²⁺ substituted compound **1** is significantly different from the rest and exhibits three transitions at ~2.43, 2.1 and 1.65 eV. These bands, probably, could be due to the splitting of 2T_2 and 2E_2 energy levels, resulting from the distortion around the Cu²⁺ ions. Such distortions in tetrahedral Cu²⁺ complexes have been reported

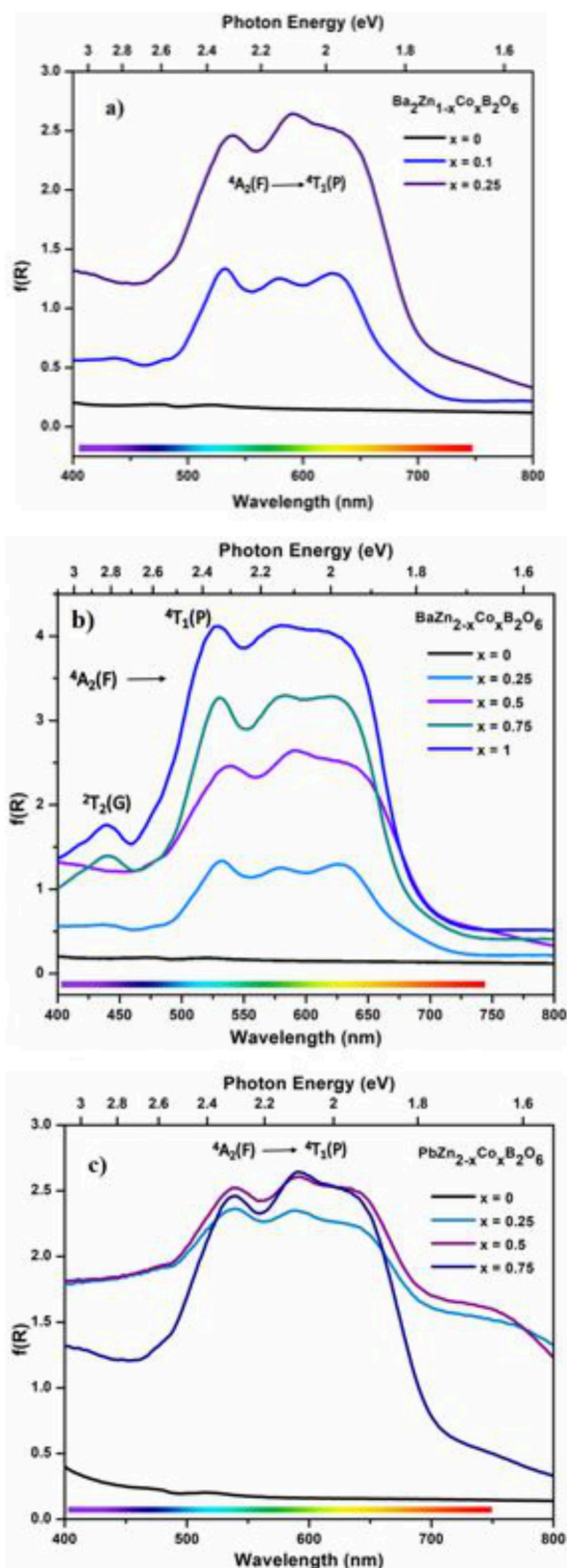


Figure 4. Optical absorption spectra of a) $Ba_2Zn_{1-x}Co_xB_2O_6$ ($0 < x \leq 0.25$); b) $BaZn_{2-x}Co_xB_2O_6$ ($0 < x \leq 1$) and c) $PbZn_{2-x}Co_xB_2O_6$ ($0 < x \leq 0.75$).

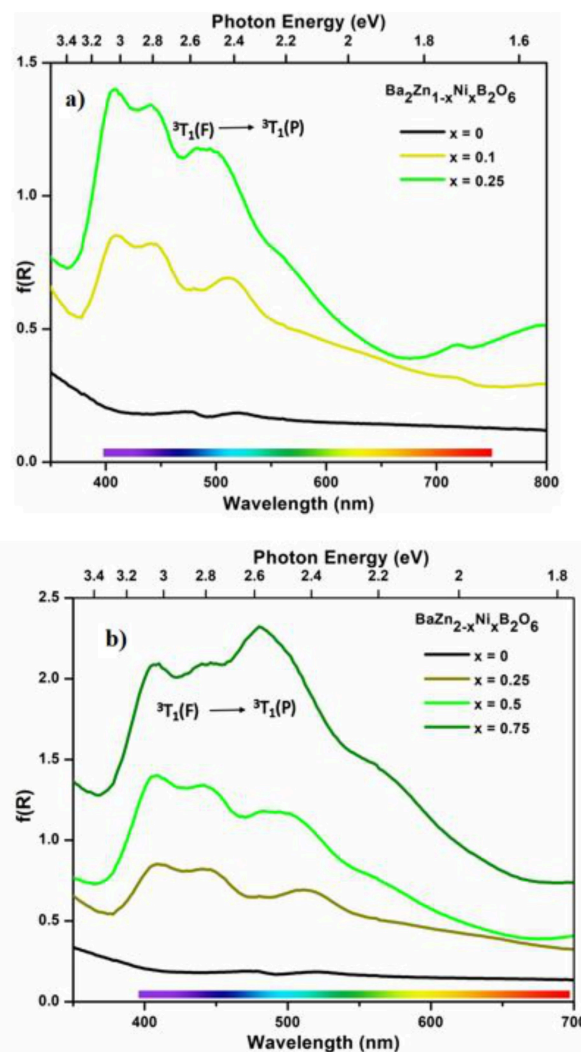


Figure 5. Optical absorption spectra of a) $Ba_2Zn_{1-x}Ni_xB_2O_6$ ($0 < x \leq 0.25$) and b) $BaZn_{2-x}Ni_xB_2O_6$ ($0 < x \leq 0.75$).

before.^[27] Thus, the maximas at ~ 2.43 , 2.1 and 1.65 eV correspond to ${}^2B_{1g} \rightarrow {}^2A_{1g}$, 2E_g and ${}^2B_{2g}$ transitions, respectively.^[28] The absorption maxima fall in the blue-green, blue and deep red regions respectively. The combination of their corresponding complementary colours might be responsible for the unusual grey colour observed in compound 1.

The Cu-compound $Pb_2CuB_2O_6$ is a dark coloured compound, and the optical absorption spectra (ESI: Figure S7) exhibits two broad absorptions, one with a maxima at ~ 1.82 eV (~ 680 nm) and the other at ~ 2.19 eV (~ 566 nm). These bands can be assigned to the spin allowed transitions: ${}^2B_{1g} \rightarrow {}^2A_{1g}$ and ${}^2B_1 \rightarrow {}^2E_g$, for the square planar Cu^{2+} ions.^[28]

Dielectric Studies

In the present study, the compounds $Ba_2ZnB_2O_6$ and $BaZn_2B_2O_6$ are formed in the non-centrosymmetric space groups, which may be attractive towards the dielectric and related properties.

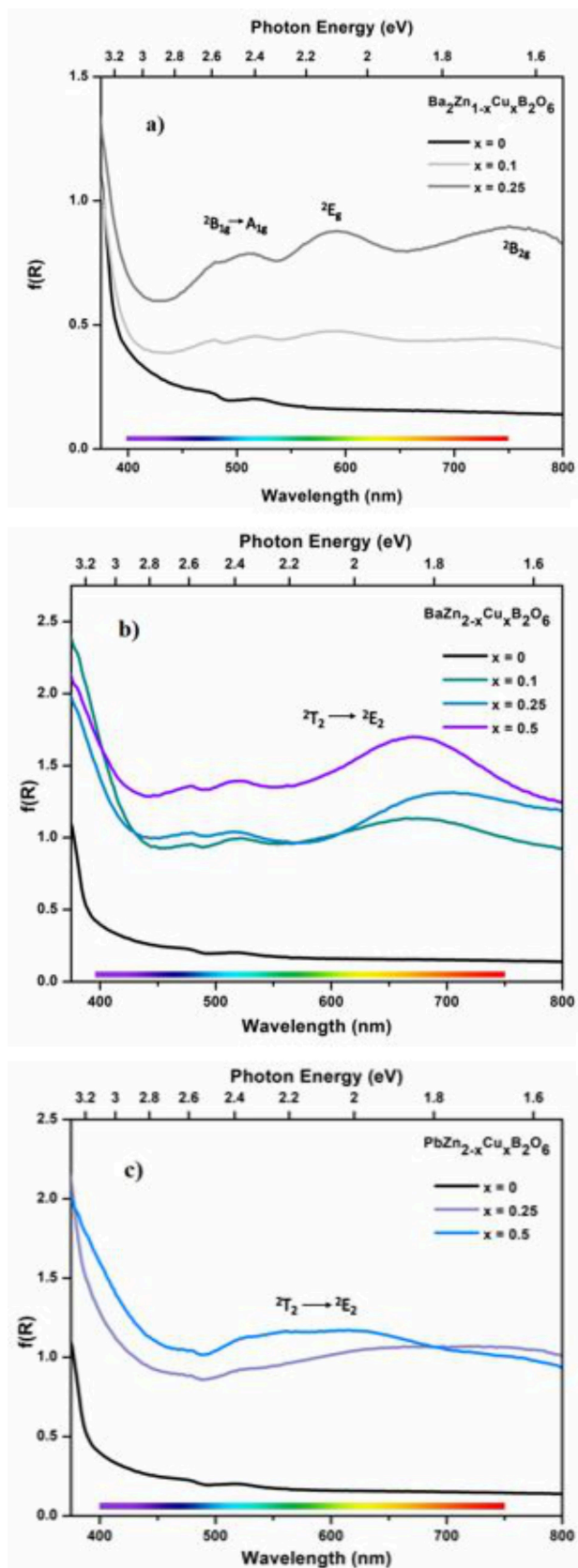


Figure 6. Optical absorption spectra of a) $\text{Ba}_2\text{Zn}_{1-x}\text{Cu}_x\text{B}_2\text{O}_6$ ($0 < x \leq 0.25$); b) $\text{BaZn}_{2-x}\text{Cu}_x\text{B}_2\text{O}_6$ ($0 < x \leq 0.5$) and c) $\text{PbZn}_{2-x}\text{Cu}_x\text{B}_2\text{O}_6$ ($0 < x \leq 0.5$).

It has been known that Pb-containing compounds also exhibit interesting dielectric behaviour as has been known for PbTiO_3 ,^[29–32] dugganite.^[20] As part of the investigations, we made attempts to substitute Pb^{2+} ions in $\text{Ba}_2\text{ZnB}_2\text{O}_6$ and also increase the Pb^{2+} concentration in $\text{PbZn}_2\text{B}_2\text{O}_6$. In both compounds, we were able to substitute 0.5Pb^{2+} ions, resulting in $(\text{Ba}_{1.5}\text{Pb}_{0.5})\text{ZnB}_2\text{O}_6$ and $(\text{Pb}_{1.5}\text{Zn}_{1.5})\text{B}_2\text{O}_6$ compounds. Thus, we investigated the dielectric behaviour at room temperature of $\text{Ba}_2\text{ZnB}_2\text{O}_6$, $(\text{Ba}_{1.5}\text{Pb}_{0.5})\text{ZnB}_2\text{O}_6$, $\text{PbZn}_2\text{B}_2\text{O}_6$, $\text{Pb}_{1.5}\text{Zn}_{1.5}\text{B}_2\text{O}_6$, $\text{BaZn}_2\text{B}_2\text{O}_6$ and $\text{Pb}_2\text{CuB}_2\text{O}_6$ (Figure 7).

The studies indicate that the compounds exhibit reasonably good dielectric behaviour with large dielectric constant values at low frequencies. The dielectric constant values, however, start to decrease on increasing the frequency to reach a value of 47 at 1000 Hz frequency. It has been known that the dielectric response changes as a function of increasing frequency due to the different polarization effects within the solid. Normally, at the low frequencies, the electronic, ionic, dipolar, and interfacial polarizations contribute to the overall polarization.^[33] On increasing the applied field, the dielectric constant values decrease due to the relaxation of the different polarizations, which is known in many ceramic oxide compounds.^[34]

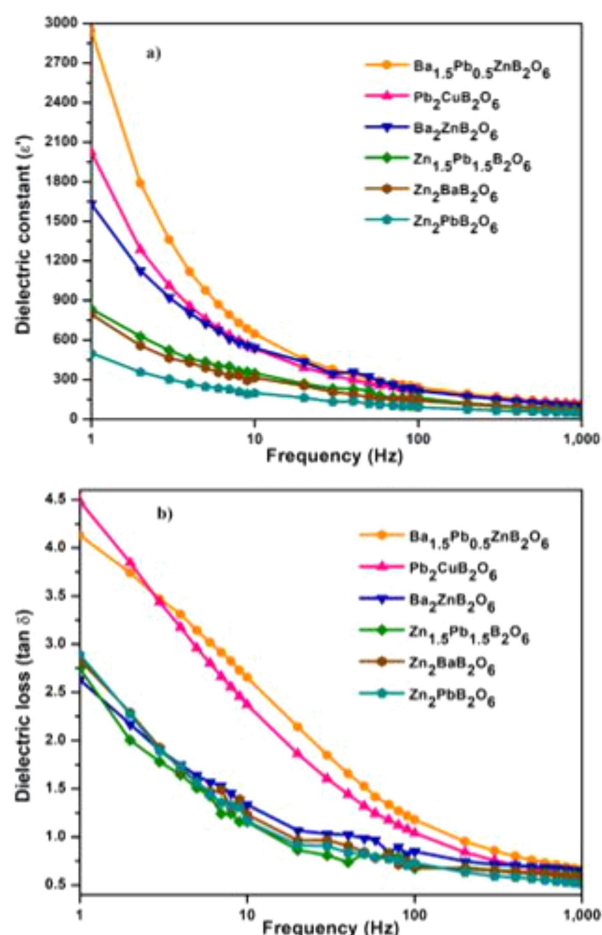


Figure 7. (a) The change in dielectric constant as a function of frequency (b) The dielectric loss as a function of frequency.

From the present study, it is clear that the Pb-containing compounds exhibit consistently higher values for the dielectric constant. The presence of 6 s^2 lone pair of electrons in Pb^{2+} ^[35] may add to distortions in the structure, which could play a role in enhancing the dielectric constant value. Thus $Ba_{1.5}Pb_{0.5}ZnB_2O_6$, stabilised in the non-centrosymmetric space group, $Pca2_1$ exhibits the highest dielectric constant value among the present compounds. We also observed that the dielectric constant values of $Pb_2CuB_2O_6$ are higher than that of $Ba_2ZnB_2O_6$. Similarly, the dielectric constant values were found to be higher in $Zn_{1.5}Pb_{1.5}B_2O_6$ compared to $PbZn_2B_2O_6$. The higher values indicate that the $6s^2$ lone pair of electrons play role in the overall dielectric behaviour of the compounds. The present studies, thus, indicate the importance of the lone pair of electrons in enhancing the dielectric behaviour in oxides.

Magnetic Studies

We have investigated the magnetic behaviour of $BaZn_{2-x}Co_xB_2O_6$ ($0.25 \leq x \leq 1$) and $Pb_2CuB_2O_6$ compounds as a function of temperature employing SQUID magnetometer in the temperature range 4.2 K–300 K.

$BaZn_{2-x}Co_xB_2O_6$ ($0.25 \leq x \leq 1$)

The temperature variation of the magnetic susceptibility (χ_m) of $BaZn_{2-x}Co_xB_2O_6$ ($0.25 \leq x \leq 1$) indicate a continuous increase in the χ_m value as a function of temperature (Figure 8). The calculated magnetic moment for various Co^{2+} concentration (ESI: Table S3) are comparable to the spin only value of $3.87 \mu_B$. The $1/\chi_m$ vs. T plot (Figure 8-inset) fitted to the Curie-Weiss law in the high temperature (HT) region (150–280 K) and low temperature (LT) region (5–50 K) resulted in negative values of Weiss constant (θ_{cw}). The negative values obtained at both the high as well as low temperature limits suggest that the

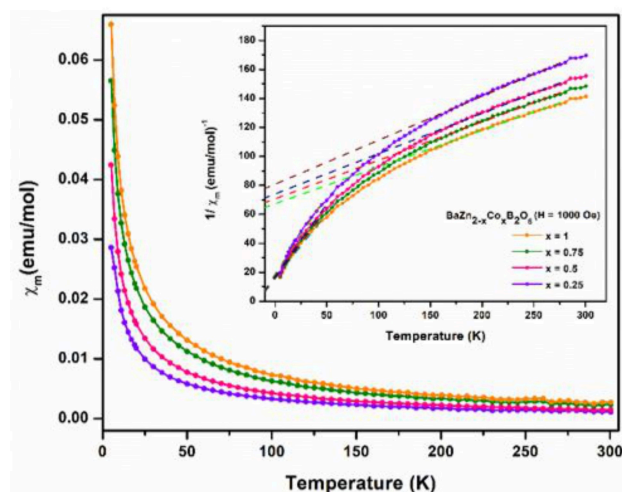


Figure 8. Magnetic susceptibility as a function of temperature for $BaZn_{2-x}Co_xB_2O_6$. Inset shows the $1/\chi_m$ -T plot.

interactions between the Co^{2+} ions are antiferromagnetic. The Curie constant values (C), fitted in the HT region are provided in ESI: Table S3. The M–H studies at 100 K and 5 K (ESI: Figure S8) also exhibited the expected behaviour.

$Pb_2CuB_2O_6$

The variation of the magnetic susceptibility (χ_m) as a function of temperature for $Pb_2CuB_2O_6$ is shown in Figure 9. The χ_m value exhibits a continuous increase as the temperature is lowered. The calculated magnetic moment at room temperature was found to be $1.46\mu_B$, which is close to the spin-only value of $1.73\mu_B$ for the uncoupled Cu^{2+} (d^9) ion. The $1/\chi_m$ vs. T plot (Inset) fitted to the Curie-Weiss law in the high temperature (HT) region (150–280 K) and also at the low temperature (LT) region (5–50 K) resulted in negative values of Weiss constant ($\theta_{cw} = -295$ K for HT and $\theta_{cw} = -13$ K for LT). The negative values at both high and low temperature limits suggest that the interactions between the Cu^{2+} ions are antiferromagnetic. The M–H plots at 300 K and 2 K also exhibited the expected behaviour (ESI: Figure S9).^[36,37]

Photoluminescence (PL) Studies

The compound $Ba_2ZnB_2O_6$ has the Ba^{2+} ions in six and seven coordination which would facilitate the substitution of rare-earth ions. The substitution of Eu^{3+} , Tb^{3+} , and Tm^{3+} ions in the host oxides, generally result in characteristic emissions in the red, green, and blue regions.^[26] Thus, we prepared a series of Eu^{3+} , Tb^{3+} and Tm^{3+} ions substituted in the $Ba_2ZnB_2O_6$ compound. The PXRD patterns of the prepared compounds indicate the formation of single-phase compounds in all the cases. Thus, $Ba_{2-x}M_xZnB_2O_6$ ($0 < x \leq 0.15$) for Eu^{3+} , ($0 < x \leq 0.09$) for Tb^{3+} and ($0 < x \leq 0.05$) for Tm^{3+} have been prepared (ESI: Figure S10).

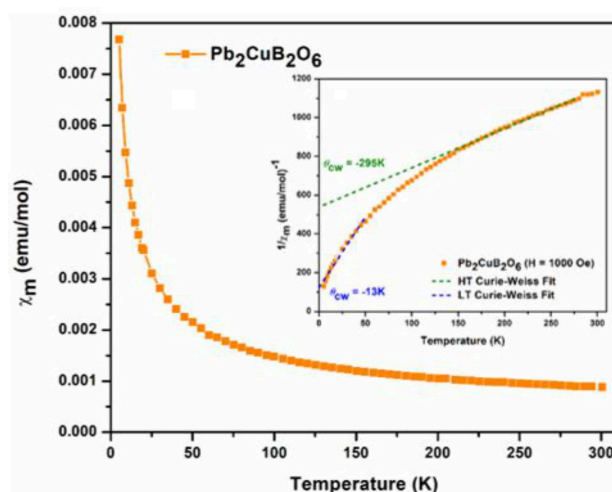


Figure 9. Magnetic susceptibility as a function of temperature for $Pb_2CuB_2O_6$. Inset shows the $1/\chi_m$ -T plot.

The photoexcitation and photoluminescence spectra of the prepared $\text{Ba}_{2-x}\text{M}_x\text{ZnB}_2\text{O}_6$ ($\text{M}=\text{Eu}^{3+}$, Tb^{3+} , Tm^{3+}) compounds are shown in Figure 10. A maximum intensity for the emission was observed at 11% for Eu, 7% for Tb and 3% for Tm substitution in the compound. Higher concentrations of these ions in $\text{Ba}_2\text{ZnB}_2\text{O}_6$ results in a reduction in the emission intensity due to the concentration caused quenching (ESI: Figure S11).

The excitation spectra of $\text{Ba}_2\text{ZnB}_2\text{O}_6$:11% Eu^{3+} (Figure 10a) exhibits the well-known excitation peaks due to the $4f-4f$ transition. Thus, the peaks observed at 362, 384, 392, 415, and 464 nm can be assigned to ${}^7\text{F}_0 \rightarrow {}^5\text{D}_4$, ${}^7\text{F}_0 \rightarrow {}^5\text{D}_4$, ${}^7\text{F}_0 \rightarrow {}^5\text{L}_7$, ${}^7\text{F}_0 \rightarrow {}^5\text{L}_6$, ${}^7\text{F}_1 \rightarrow {}^5\text{D}_3$, and ${}^7\text{F}_0 \rightarrow {}^5\text{D}_2$ transitions of the Eu^{3+} ions, respectively.^[38] We have employed the maximum intensity peak (392 nm) as the excitation wavelength for examining the luminescence of Eu^{3+} ions. On excitation using 392 nm wavelength, the emission spectrum exhibits strong red-luminescence with peaks at 536, 590, 616, 648, and 699 nm, which can be assigned to ${}^5\text{D}_0 \rightarrow {}^7\text{F}_J$ ($J=0, 1, 2, 3$, and 4) transitions of the Eu^{3+} ions, respectively.^[39] From the emission intensity as a function of the concentration of Eu^{3+} ions in $\text{Ba}_2\text{ZnB}_2\text{O}_6$, we observed a maximum at ~11% Eu^{3+} substitution (ESI: S11a).

The substitution of the Tb^{3+} ions in $\text{Ba}_2\text{ZnB}_2\text{O}_6$ (Figure 10b) also resulted in excitation peaks in the 280–400 nm wavelength range which can be assigned to the known $f-f$ transitions of the Tb^{3+} ions,^[40] with the maximum intense peak at 379 nm. Thus,

we employed 379 nm wavelength for investigating the luminescence of Tb^{3+} ions. The emission spectra exhibited strong green luminescence along with weak red emissions. The observed strong emission peaks are: 514 nm (${}^5\text{D}_4 \rightarrow {}^7\text{F}_6$), 542 nm (${}^5\text{D}_4 \rightarrow {}^7\text{F}_5$) in the green region and weak emissions at 582 nm (${}^5\text{D}_4 \rightarrow {}^7\text{F}_4$) and 619 nm (${}^5\text{D}_4 \rightarrow {}^7\text{F}_3$) in the red region.^[39] For the Tb^{3+} ions substitution, we observed the maximum emission intensity at ~7% Tb^{3+} substitution (ESI: Figure S11b).

The Tm^{3+} ions substitution in $\text{Ba}_2\text{ZnB}_2\text{O}_6$ (Figure 11c) exhibited a single sharp absorption peak at 360 nm, which corresponds to the ${}^3\text{H}_6 \rightarrow {}^1\text{D}_2$ transition.^[41] On excitation with 360 nm wavelength, the emission spectrum exhibited a strong band at 453 nm, which can be assigned to the ${}^1\text{D}_2 \rightarrow {}^3\text{F}_4$ transition.^[42] In addition, weaker emission bands were observed at 490 nm, 590 nm and 685 nm which can be assigned to the ${}^1\text{G}_4 \rightarrow {}^3\text{H}_6$, ${}^1\text{D}_2 \rightarrow {}^3\text{H}_4$, and ${}^1\text{G}_4 \rightarrow {}^3\text{F}_4$ transitions.^[43] The energy levels of the Tm^{3+} substituted compounds have been known to exhibit complex emissions due to the Russell-Saunders (R-S) coupling. The relaxation of the excited states of Tm^{3+} ions can occur through different pathways, which gives rise to ultra-violet, visible as well as infrared emissions.^[44] Our studies indicates that the maximum emission intensity results for 3% Tm^{3+} substitution (ESI: Figure S11c).

From the PL studies, we established that the substitution of Eu^{3+} (red), Tb^{3+} (green), Tm^{3+} (blue) ions gives rise to intense and characteristic emissions. The corresponding chromaticity diagram for the different phosphors are shown in Figure 11 and the corresponding CIE (Commission Internationale de L'Eclairage) coordinates are given in Table 2.

In the present study, we have achieved the three important color emissions (Red, Green, and Blue; RGB), which suggested that the concentrations of the phosphors can be optimized to result in white light emission. For this, we have fixed the dopant concentrations Tm^{3+} at 1% and Tb^{3+} at 2% and changed the concentration of Eu^{3+} ions. Thus, we have prepared a series of $\text{Ba}_2\text{ZnB}_2\text{O}_6$:1% Tm^{3+} , 2% Tb^{3+} , $x\%$ Eu^{3+} ($x=0, 0.5, 1.0, 2.0, 3.0, 4.0$) samples. The PL spectra ($\lambda_{\text{ex}}=360$ nm) of the compounds

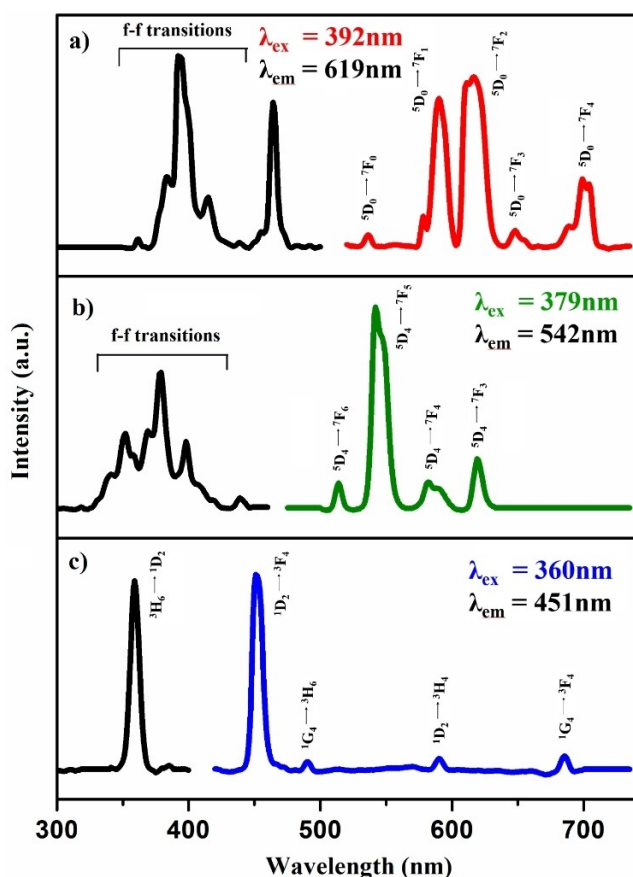


Figure 10. The excitation and emission spectra of a) $\text{Ba}_2\text{ZnB}_2\text{O}_6$: 11% Eu^{3+} , b) $\text{Ba}_2\text{ZnB}_2\text{O}_6$: 7% Tb^{3+} and c) $\text{Ba}_2\text{ZnB}_2\text{O}_6$: 3% Tm^{3+} samples.

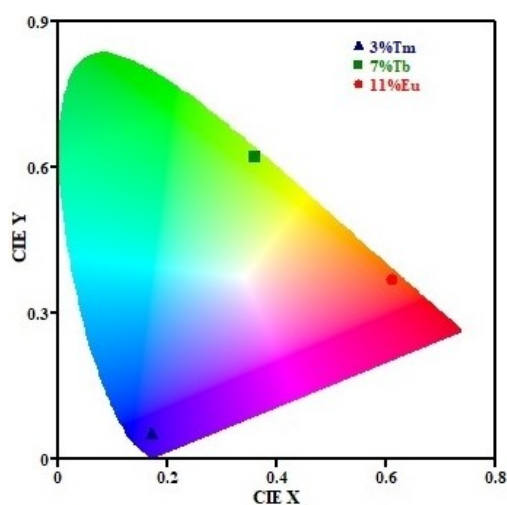


Figure 11. CIE diagram of $\text{Ba}_2\text{ZnB}_2\text{O}_6$ substituted independently with 3% Tm^{3+} , 7% Tb^{3+} , and 11% Eu^{3+} . Note that the emission is observed in the blue, green and red regions.

Table 2. CIE chromaticity coordinates for Ba₂ZnB₂O₆ compounds with 3% Tm³⁺, 7% Tb³⁺, and 11% Eu³⁺ samples.

Compound	x	y	CCT (K)
Ba ₂ ZnB ₂ O ₆ : 11% Eu ³⁺	0.61	0.37	1862
Ba ₂ ZnB ₂ O ₆ : 3% Tm ³⁺	0.17	0.05	1715
Ba ₂ ZnB ₂ O ₆ : 7% Tb ³⁺	0.36	0.62	5089

and the corresponding CIE chromaticity diagram are presented in Figures 12 and 13 and Table S4. We observed white light emission at $x=1.0$ of Eu³⁺ ions. Thus, we have obtained a single-phase white-light-emitting phosphor by carefully adjusting the blue (Tm³⁺), green (Tb³⁺) and red (Eu³⁺) emissions in Ba₂ZnB₂O₆ host.

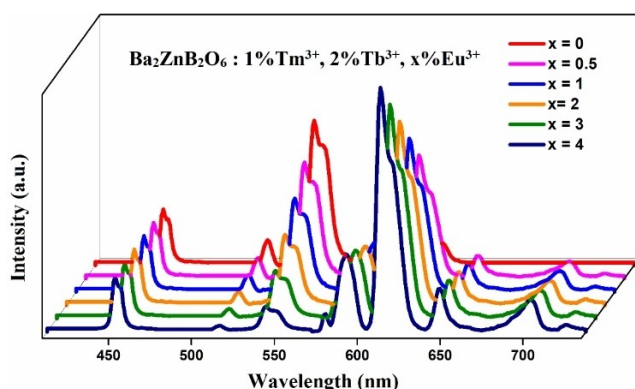


Figure 12. PL emission spectra of Ba₂ZnB₂O₆: 1% Tm³⁺, 2% Tb³⁺, x% Eu³⁺ samples ($\lambda_{\text{exc}}=360$ nm), recorded at room temperature.

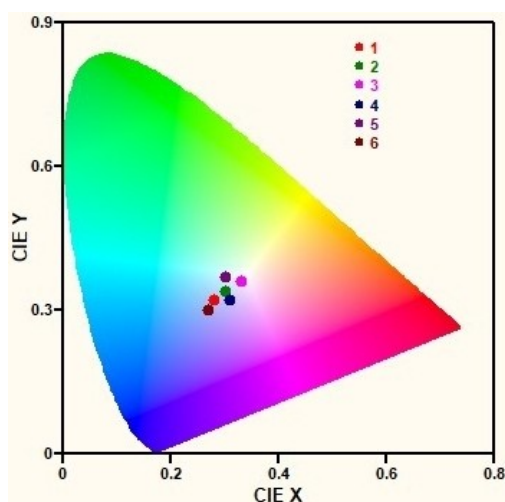


Figure 13. CIE colour coordinate diagram for Ba₂ZnB₂O₆: 1% Tm³⁺, 2% Tb³⁺, x% Eu³⁺ samples with different Eu³⁺ concentrations ($0 < x < 4.0$). Note that the white-light emission is observed for Eu³⁺ concentration of 1%.

Catalytic Studies

The hydroxylation of aromatic moieties to the corresponding phenols is important in synthetic organic chemistry. The well-known synthesis of phenols by Hock process resulted in poorer yield.^[45] The phenols are synthesized through a nucleophilic substitution of aryl halides,^[46] hydroxylation of benzyne intermediates,^[47] and hydrolysis of arene diazonium salts,^[48] The above approaches were shown to have poor functional group compatibility and narrow substrate scope, which limits their usefulness and applicability.^[49] In recent times, ipso-hydroxylation is being pursued as an alternate strategy.^[50]

Ipsso-hydroxylation involves the oxidation of aryl boronic acid in the presence of H₂O₂ and a catalyst.^[51] In the present study, we have performed the ipso-hydroxylation reaction of arylboronic acid to the corresponding phenol employing Pb₂CuB₂O₆ as the catalyst in the presence of H₂O₂ (ESI: Procedure S1).

The catalytic reaction conditions for the ipso-hydroxylation of arylboronic acids were standardised with respect to the solvent, amount of catalyst, time of reaction etc. The studies indicated the highest yield (~98%) when THF was employed as the solvent along with H₂O₂ (ESI: Table S5).

As part of the study, we have examined the role of substituents on arylboronic acids (Table 3). We observed that the electron donating groups, substituted at the para-position, gives better yields compared to the substitution at the meta or ortho positions. This observation appears to be the same with respect to the electron-withdrawing groups as well. In addition, the present studies indicate that the ipso-hydroxylation was selective and successful in the presence of other substituents such as nitrile, carbonyl, ester, formyl as well as secondary amine (Table 3).

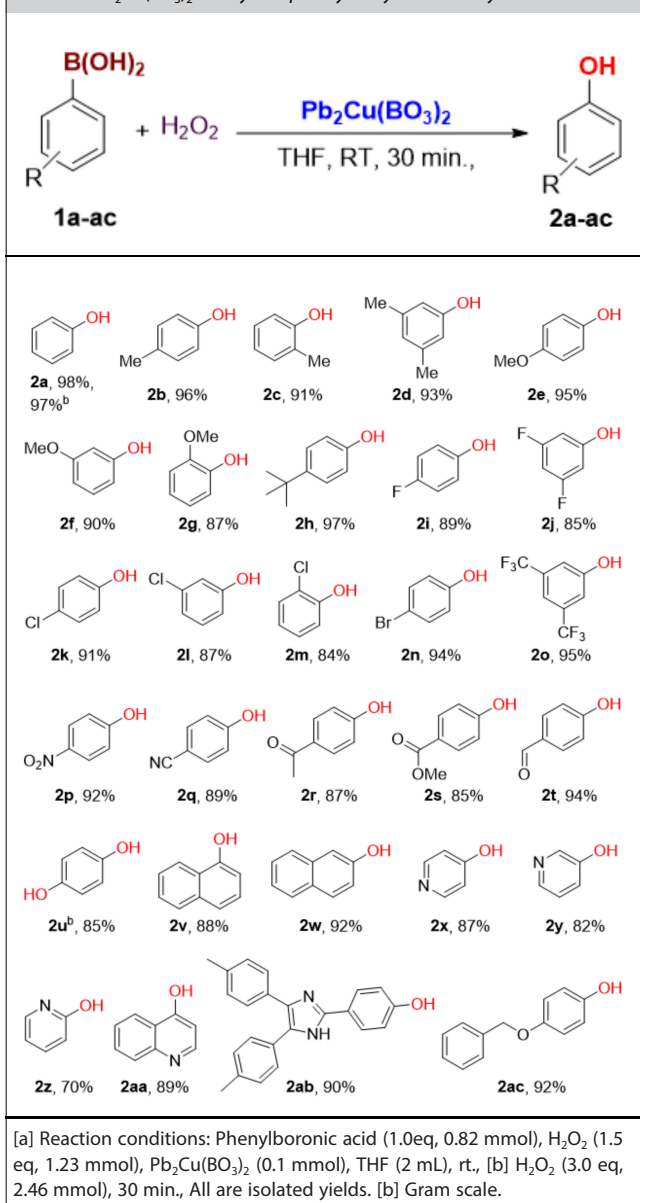
We have also explored this reaction with other Cu-salts under identical reaction conditions (ESI: Table S6). While the nitrate, acetate and sulphate salts resulted in a moderate yield of ~40–60% (Table S6, Entries 1–3), the halide salts were found to be inactive as the catalyst with negligible formation of the desired product (Table S6, entries 4–6).

We have carried out the catalytic reaction over other transition metal substituted Ba₂ZnB₂O₆, BaZn₂B₂O₆ and PbZn₂B₂O₆ compounds (ESI: Table S7). In all the cases, the yields were found to be smaller compared to what was observed for Pb₂CuB₂O₆.

We have observed that the Pb₂CuB₂O₆ catalyst was reusable for up to seven cycles without any perceptible loss in the catalytic activity (ESI: Figure S12). The SEM images as well as PXRD patterns of the catalyst before and after catalytic studies indicated that the catalyst is stable under the reaction conditions with no change in the crystallinity (ESI: Figures S13 and S14).

The hot filtration test was carried out, wherein the catalyst was removed from the reaction mixture after a time period of 20 mins, and after that the product formation was not observed (ESI: Figure S15). This indicates that the reaction proceeds catalytically. A plausible mechanism for the ipso-hydroxylation

Table 3. $\text{Pb}_2\text{Cu}(\text{BO}_3)_2$ catalyzed *ipso*-hydroxylation of arylboronic acids.^[a]



has been proposed, which is based on other studies (ESI: Scheme 1).^[52]

Conclusions

Four compounds, $\text{Ba}_2\text{ZnB}_2\text{O}_6$, $\text{BaZn}_2\text{B}_2\text{O}_6$, $\text{PbZn}_2\text{B}_2\text{O}_6$ and $\text{Pb}_2\text{CuB}_2\text{O}_6$, related to the kotoite structure has been synthesized and characterized. Attempts to substitute divalent transition elements in place of Zn^{2+} ions were partially successful resulting in new-colored compounds. The optical absorption spectra could be explained based on the Tanabe-Sugano diagram and corresponding d-d transition. The dielectric studies indicate that Pb^{2+} -containing compounds exhibit consistently higher values, especially at low frequencies. Magnetic studies suggest the compounds, $\text{BaZnCoB}_2\text{O}_6$ and $\text{Pb}_2\text{CuB}_2\text{O}_6$, exhibit

anti-ferromagnetic behaviour. The compound $\text{Ba}_2\text{ZnB}_2\text{O}_6$ was found to be a good host for observing rare-earth luminescence giving rise to intense red (Eu^{3+}), green (Tb^{3+}) and blue (Tm^{3+}) emissions. Suitable modifications on the substitution of these three different phosphors resulted in a compound, exhibiting white-light emission. The $\text{Pb}_2\text{CuB}_2\text{O}_6$ compound was found to be a good heterogenous catalyst for the ipso-hydroxylation of arylboronic acids. The many desirable properties exhibited by the kotoite-related compounds in the present study suggests there is a need to explore the other mineral structures further towards new material.

Experimental Section

The synthesis of all the compounds was carried out employing conventional solid-state technique. Stoichiometric mixtures of the starting materials were heated in air for 36 h at 600 °C to 850 °C, with intermittent grindings. The synthesis conditions along with the list of the prepared compounds is given in ESI (Table S1).

All the prepared compounds were characterized employing Powder X-Ray Diffraction (PXRD). The PXRD patterns were recorded employing Panalytical EMPYREAN diffractometer (Ni-filtered Cu K α radiation, $\lambda = 1.5406 \text{ \AA}$), at room temperature in the 2θ range 10–80° with a step size of 0.02° and a step duration of 60s. The collected PXRD data were refined using the GSAS II program.^[14] Lattice parameters, scale factors, background (Fourier polynomial background function), pseudo-Voigt (U, V, W, and X), and isothermal temperature factors (U_{iso}) were refined. Thermal parameters were constrained to be the same for different atoms occupying the same sites. The simulation of the theoretical PXRD patterns were carried out employing POWDERCELL program.^[15] The UV-Vis-NIR reflectance spectra for all the compounds were recorded using the PerkinElmer Lambda950 UV/Vis double-beam spectrometer (spectral range = 200–2500 nm). Dielectric measurements were carried out using a Novocontrol impedance analyser (Alpha-A) in the frequency range 0.1 Hz–1 MHz at room temperature. Magnetic studies were carried out in the temperature range 4.2 K–300 K by using the SQUID magnetometer (QuantumDesign, USA). SEM images were recorded with JEOL SEM IT 300 scanning electron microscope.

Acknowledgements

SN thanks the Science and Engineering Research Board (SERB), Government of India, for the award of a J. C. Bose National Fellowship. SERB, Government of India is also thanked for the award of a research grant (S.N.). We are thankful to Prof. Rajeev Ranjan for his generous help with the dielectric measurements. I thank Indian Institute of Science (IISc) for research fellowship and research facilities.

Conflict of Interests

The authors declare no conflict of interest.

Data Availability Statement

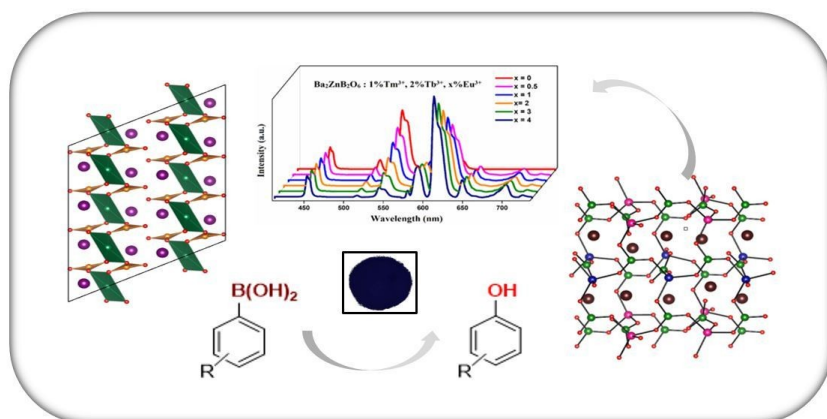
The data that support the findings of this study are available in the supplementary material of this article.

Keywords: Kotoite · Dielectric · Magnetism · White light emission · Organic catalysis

- [1] a) P. C. Burns, J. D. Grice, F. C. Hawthorne, *Can. Miner.* **1995**, *33*, 1131–1151; b) F. C. Hawthorne, P. C. Burns, J. D. Grice, *Rev. Miner.* **1996**, *33*, 41–116.
- [2] a) J. D. Grice, P. C. Burns, F. C. Hawthorne, *Can. Miner.* **1999**, *37*, 731–762; b) N. I. Leonyuk, V. V. Maetsev, E. V. Volkova, *Molecules* **2020**, *25*, 2450.
- [3] R. Bubnova, S. Volkov, B. Albert, S. Filatov, *Crystals* **2017**, *7*, 93.
- [4] a) M. Mutalipu, K. R. Poeppelmeier, S. Pan, *Chem. Rev.* **2021**, *121*, 1130–1202; b) O. D. Abodurin, K. E. Mabrouk, M. Bricha, *J. Mater. Chem. B.* **2023**, *11*, 955; c) P. Becker, *Adv. Mater.* **1998**, *10*, 979–992.
- [5] a) J. P. Atfield, A. M. T. Bell, L. M. Rodriguez-Martinez, J. M. Greneche, R. Retoux, R. J. Cernik, J. F. Clarke, D. A. Perkins, *J. Mater. Chem.* **1999**, *9*, 205–209; b) X. Chen, J. Zhang, W. Xiao, X. Song, *RSC Adv.* **2023**, *13*, 16272; c) Y. Lin, G. E. Wang, C. L. Hu, J. H. Feng, L. N. Li, J. G. Mao, *Angew. Chem. Int. Ed.* **2019**, *58*, 13390–13393.
- [6] T. B. Bekker, V. P. Solntsev, S. V. Rashchenko, A. P. Yelissev, A. V. Davydov, A. A. Kragzhda, A. E. Kokh, A. B. Kuznetsov, S. Park, *Inorg. Chem.* **2018**, *57*(5), 2744–2751.
- [7] H. F. J. Glass, Z. Liu, P. M. Bayley, E. Suard, S. H. Bo, P. G. Khalifah, C. P. Grey, S. E. Dutton, *Chem. Mater.* **2017**, *29*(7), 3118–3125.
- [8] a) C. Friedel, E. Frémy, *Ann. Chim. Phys.* **1851**, *33*, 50; b) C. Friedel, E. Frémy, *Comptes Rendus Chim.* **1887**, *105*, 1263.
- [9] G. Sivakumar, S. Natarajan, *Z. Anorg. Allg. Chem.* **2022**, *648*, 1–7, e202200017.
- [10] R. W. Smith, L. J. Koliha, *Mater. Res. Bull.* **1994**, *29*, 1203–1210.
- [11] R. W. Smith, D. A. Keszler, *J. Solid State Chem.* **1992**, *100*, 325–330.
- [12] S. Pan, J. P. Smit, M. R. Marvel, C. L. Stern, B. Watkins, K. R. Poeppelmeier, *Mater. Res. Bull.* **2006**, *41*, 916–924.
- [13] X. A. Chen, Y. H. Zhao, X. A. Chang, L. Zhang, H. P. Xue, *Acta Cryst.* **2006**, *62*, 11–12.
- [14] B. H. Toby, R. B. V. Dreele, *J. Appl. Cryst.* **2013**, *46*, 544–549.
- [15] W. Kraus, G. Nolze, *J. Appl. Crystallogr.* **1996**, *29*, 301–303.
- [16] P. Kubelka, F. Munk, *Z. Technol. Phys.* **1931**, *12*, 593–601.
- [17] A. K. Cheetham, G. Ferey, T. Loiseau, *Angew. Chem. Int. Ed.* **1999**, *38*, 3268–3292.
- [18] A. Bhim, J. P. Sutter, J. Gopalakrishnan, S. Natarajan, *Chem. Eur. J.* **2021**, *27*, 1995–2008.
- [19] A. Bhim, S. Laha, J. Gopalakrishnan, S. Natarajan, *Chem. Asian J.* **2017**, *12*, 2734–2743.
- [20] A. Bhim, W. Zhang, P. S. Halasyamani, J. Gopalakrishnan, S. Natarajan, *Inorg. Chem.* **2019**, *58*, 8560–8569.
- [21] A. B. P. Lever, *Inorganic Electronic Spectroscopy*, Elsevier, Amsterdam **1968**.
- [22] S. Tamilarasan, M. L. P. Reddy, S. Natarajan, J. Gopalakrishnan, *Chem. Asian J.* **2016**, *11*, 3234–3240.
- [23] H. Berke, *Chem. Soc. Rev.* **2007**, *36*, 15–30.
- [24] M. Dondi, M. Ardit, G. Cruciani, C. Zanelli, *Am. Miner.* **2014**, *99*, 1736–1745.
- [25] G. Costa, M. J. Ribeiro, W. Hajjaji, M. P. Seabra, J. A. Labrincha, M. Dondi, G. Cruciani, *J. Eur. Ceram. Soc.* **2009**, *29*, 2671–2678.
- [26] T. C. Brunold, H. U. Gudel, E. Cavalli, *Chem. Phys. Lett.* **1997**, *268*, 413–420.
- [27] a) A. Kyono, A. S. Gramsch, Y. Nakamoto, M. Sakata, M. Kato, T. Tamura and T. Yamanaka, *Am. Miner.* **2015**, *100*, 1335652; b) M. R. Suchomel, D. P. Shoemaker, L. Ribaud, M. C. Kemei, R. Sheshadri, *Phys. Rev. B* **2012**, *86*, 054406; c) B. J. Kennedy, Q. Zhou, *J. Solid State Chem.* **2008**, *181*, 2227–2230.
- [28] L. Binet, J. Lizion, S. Bertaina, D. Gourier, *J. Phy. Chem. C* **2021**, *125*, 25189–25196.
- [29] H. Lemziouka, L. E. H. Omari, R. Moubah, A. Boutahar, S. Bahhar, M. Abid, H. Lassri, *Mater. Today. Proc.* **2021**, *37*, 3940–3945.
- [30] E. H. Lahrar, O. El Ghadraoui, M. Zouhairi, A. Harrach, T. Lamcharfi, E. H. El Ghadraoui, *New. J. Chem.* **2021**, *45*, 13293.
- [31] V. G. Bhide, K. G. Deshmukh, M. S. Hegde, *Physica* **1962**, *28*, 871–876.
- [32] V. A. Chaudhari, G. K. Bichile, *Smart Mater. Res.* **2013**, ID: 147524; pages 9.
- [33] B. Quan, X. Liang, G. Ji, Y. Cheng, W. Liu, J. Ma, Y. Zhang, D. Li, G. Xu, *J. Alloys Compd.* **2017**, *728*, 1065–1075.
- [34] G. Blasse, *J. Inorg. Nucl. Chem.* **1965**, *27*, 993–1003.
- [35] A. R. Makhdoom, M. J. Akhtar, M. A. Rafiq, M. Siddique, M. Iqbal, M. M. Hasan, *AIP Adv.* **2014**, *4*, 037113.
- [36] R. E. Newnham, R. P. Santoro, P. F. Seal, G. R. Stallings, *Phys. Status Solidi* **1966**, *16*, K17–K19.
- [37] N. V. Kazak, M. S. Platonov, N. B. Ivanova, Y. V. Knyazev, L. N. Bezmaternykh, E. V. Eremin, A. D. Vasil'Ev, O. A. Bayukov, S. G. Ovchinnikov, D. A. Velikanov, Y. V. Zubavichus, *J. Exp. Theor. Phys.* **2013**, *117*, 94–107.
- [38] a) Q. Zhang, X. Wang, X. Ding and Y. Wang, *Inorg. Chem.* **2017**, *56*, 6990–6998; b) M. N. Luwang, R. S. Ningthoujam, S. K. Srivastava and R. K. Vatsa, *J. Am. Chem. Soc.* **2011**, *133*, 2998–3004.
- [39] Y. Liu, X. Rong, M. Li, M. Molokeev, J. Zhao, Z. Xia, *Angew. Chem.* **2020**, *59*, 11634–11640.
- [40] a) L. Hou, S. Cui, Z. Fu, Z. Wu, X. Fu, J. H. Jeong, *Dalton Trans.* **2014**, *43*, 5382–5392; b) Y. Jin, Y. Hu, L. Chen, X. Wang, G. Ju and Z. Mu, *J. Lumin.* **2013**, *138*, 83–88; c) D. Liu, Y. Jin, Y. Lv, G. Ju, C. Wang, L. Chen, W. Luo, Y. Hu, *J. Am. Ceram. Soc.* **2018**, *101*, 5627–5639; d) R. Li, Y. Liu, N. Zhang, L. Li, L. Liu, Y. Liang, S. Gan, *J. Mater. Chem. C* **2015**, *3*, 3928–3934.
- [41] G. Li, C. Li, C. Zhang, Z. Cheng, Z. Quan, C. Peng, J. Lin, *J. Mater. Chem.* **2009**, *19*, 8936–8943.
- [42] J. Li, Q. Liang, J.-Y. Hong, J. Yan, L. Dolgov, Y. Meng, Y. Xu, J. Shi, M. Wu, *ACS Appl. Mater. Interfaces* **2018**, *10*, 18066–18072.
- [43] L. Marek, M. Sobczyk, W. Wrzeszcz, *J. Rare Earths* **2019**, *37*, 1188–1195.
- [44] a) L. Wu, Y. Zhang, M. Gui, P. Lu, L. Zhao, S. Tian, Y. Kong, J. Xu, *J. Mater. Chem.* **2012**, *22*, 6463–6470; b) T. Grzyb, A. Szczeszak, J. Rozowska, J. Legendziewicz, S. Lis, *J. Phys. Chem. C* **2012**, *116*, 3219–3226.
- [45] A. Knop, V. Böhmer, L. A. Pilato, *Compr. Polym. Sci. Suppl.* **1989**, *5*, 611–647.
- [46] a) T. Ikawa, K. W. Anderson, R. E. Tundel, S. L. Buchwald, *J. Am. Chem. Soc.* **2006**, *128*, 10694–10695; b) D. Zhao, N. Wu, S. Zhang, P. Xi, X. Su, J. Lan, J. You, *Angew. Chem. Int. Ed.* **2009**, *48*, 8729–8732.
- [47] T. George, R. Mabon, G. Sweeney, J. B. Sweeney, A. Tavassoli, *J. Chem. Soc. Perkin Trans.* **2000**, *1*, 2529–2574.
- [48] a) J. P. Lambooy, *J. Am. Chem. Soc.* **1950**, *72*, 5327–5328; b) T. Cohen, A. G. Dietz Jr., J. R. Miser, *J. Org. Chem.* **1977**, *42*, 2053–2058.
- [49] K. Inamoto, K. Nozawa, M. Yonemoto, Y. Kondo, *Chem. Commun.* **2011**, *47*, 11775–11777.
- [50] S. K. Das, M. Tahu, M. Gohain, D. Deka, U. Bora, *Sustainable Chem. Pharm.* **2020**, *17*, 100296.
- [51] P. Gogoi, P. Bezboruah, J. Gogoi, R. C. Boruah, *Eur. J. Org. Chem.* **2013**, *32*, 7291–7294.
- [52] C. K. Prier, D. A. Rankic, D. W. C. Macmillan, *Chem. Rev.* **2013**, *113*, 5322–5363.

Manuscript received: July 22, 2024
Revised manuscript received: October 24, 2024
Accepted manuscript online: November 7, 2024
Version of record online: ■■, ■■

RESEARCH ARTICLE



S. Sasmal, N. Devarajan, S. Natarajan*

1 – 12

Synthesis, Structure and Properties of Compounds Derived from Kotoite-related Structures: $A_2MB_2O_6$ (A = Zn, Ba, Pb; B = Pb, Ba, Zn, Cu)

New members of kotoite-related mineral structures were prepared and characterized. The compound, $Ba_2ZnB_2O_6$ was found to be a good host for rare-earth luminescence and white-light emission. The substitution of transition elements in these oxides

gives rise to new colored materials, which may be attractive candidates for new inorganic pigments. The compound $Pb_2CuB_2O_6$ exhibits heterogeneous catalysis for the ipso-hydroxylation of arylboronic acids.